Journal of Applied Physics

Melts of single-chain nanoparticles: A neutron scattering investigation

Cite as: J. Appl. Phys. **127**, 044305 (2020); https://doi.org/10.1063/1.5140705
Submitted: 30 November 2019 . Accepted: 10 January 2020 . Published Online: 28 January 2020

Arantxa Arbe, Jon Rubio, Paula Malo de Molina, Jon Maiz, José A. Pomposo, Peter Fouquet, Sylvain Prevost, Fanni Juranyi, Marina Khaneft, and Juan Colmenero

AIP Publishing

Journal of Applied Physics ARTICLE scitation.org/journal/jap

Melts of single-chain nanoparticles: A neutron scattering investigation

Cite as: J. Appl. Phys. **127**, 044305 (2020); doi: 10.1063/1.5140705
Submitted: 30 November 2019 · Accepted: 10 January 2020 ·
Published Online: 28 January 2020

Arantxa Arbe,[1,a)] Jon Rubio,[1] Paula Malo de Molina,[1,b)] Jon Maiz,[1,b)] José A. Pomposo,[1,c)] Peter Fouquet,[2] Sylvain Prevost,[2] Fanni Juranyi,[3] Marina Khaneft,[4] and Juan Colmenero[1,d)]

AFFILIATIONS

[1]Centro de Física de Materiales (CFM) (CSIC–UPV/EHU)—Materials Physics Center (MPC), Paseo Manuel de Lardizabal 5, 20018 San Sebastián, Spain
[2]Institut Laue–Langevin, BP 156, 38042 Grenoble Cedex 9, France
[3]Laboratory for Neutron Scattering, Paul Scherrer Institut, CH-5232 Villigen, Switzerland
[4]Jülich Centre for Neutron Science (JCNS), Forschungszentrum Jülich GmbH, Outstation at MLZ, Lichtenbergstraße 1, 85747 Garching, Germany

Note: This paper is part of the Special Topic on: Polymer-Grafted Nanoparticles.

[a)]**Author to whom correspondence should be addressed:** a.arbe@ehu.eus
[b)]IKERBASQUE—Basque Foundation for Science, María Díaz de Haro 3, 48013 Bilbao, Spain.
[c)]Departamento de Física de Materiales (UPV/EHU), Apartado 1072, 20080 San Sebastián, Spain; IKERBASQUE—Basque Foundation for Science, María Díaz de Haro 3, 48013 Bilbao, Spain.
[d)]Departamento de Física de Materiales (UPV/EHU), Apartado 1072, 20080 San Sebastián, Spain; Donostia International Physics Center, Paseo Manuel de Lardizabal 4, 20018 San Sebastián, Spain.

ABSTRACT

The impact of purely intramolecular cross-linking on the properties of a polymer melt is studied by neutron diffraction and quasielastic incoherent and coherent neutron scattering on a system composed exclusively of single-chain nanoparticles. As a reference, a parallel study is presented on the melt of the linear precursor chains' counterpart. Associated with structural heterogeneities provoked by the internal compartmentalization due to cross-links, a dramatic slowing down of the relaxation of density fluctuations is observed at intermediate length scales.

I. INTRODUCTION

Single-chain nanoparticles (SCNPs) are nano-objects obtained by intramolecular cross-linking of individual macromolecular chains. Due to their ultrasmall size, softness, and internal compartmentalization, they are believed to be a fundamental ingredient in the field of nanotechnology.[1] Concerning practical applications of SCNPs, several proof-of-concept experiments have confirmed their potential use in catalysis, biosensing, bioimaging, protein mimicry, drug delivery, and all-polymer nanocomposites, among other applications. For instance, metalloenzyme mimetic SCNPs showed enhanced catalytic activity[2] and selectivity[3] toward a variety of chemical compounds, as well as in some cases catalyst recyclability.[4] Moreover, SCNPs can be used as nanoreactors for the synthesis of other nanomaterials (e.g., gold nanoparticles[5] and quantum dots[6]) and even synthetic macromolecules (e.g., water-soluble polymers[7] and intrinsically conducting polymers[8]) or as templates for the synthesis of fluorescent carbon nanodots[9] as well as reversible nanocontainers for CO_2 storage.[10] Several SCNPs are able to sense metal ions[11] and even proteins.[12] A variety of SCNP systems have been designed and constructed for bioimaging (e.g., magnetic resonance imaging,[13] single photon emission computerized tomography,[14] and fluorescence imaging[15]) and drug delivery applications (e.g., controlled delivery of chiral amino acid derivatives,[16] peptides,[17] vitamins,[18] and drugs[19]). Also, SCNPs have been employed for the development of all-polymer nanocomposites.[1,20] In addition to such applied interest, SCNPs can be considered

model macromolecules to address basic questions on the effect of chain topology on the material properties. For instance, a system composed exclusively of SCNPs realizes the situation of a purely intramolecularly cross-linked polymer bulk. Thus, investigations on a melt of SCNPs can help address one fundamental question: What is the impact of the chain topology on the properties of a polymeric material and, in particular, how does it behave if cross-links are of purely intramolecular character? This basic question also arises motivated by previous results obtained on a nanocomposite consisting of SCNPs embedded in a matrix of flexible linear chains.[21–23] There, a clear impact of the presence of SCNPs was found on the dynamics of the matrix at different levels (glass-transition, Rouse dynamics, and, particularly striking, on the entanglements).

In this work, we present a neutron scattering investigation on melts of SCNPs. Neutron scattering provides spatial resolution through the scattering vector (Q) dependence of the measured magnitudes. Energy-resolved experiments have been applied to both protonated and perdeuterated systems to follow self-atomic (hydrogen) and collective motions, respectively. Complementary neutron diffraction has revealed the structural features. A bulk sample composed of the long linear counterpart chains (precursor macromolecules without cross-links) has also been investigated as a reference. Our study demonstrates that the structural and dynamical properties at local length scales including the intermolecular distances (in particular, the structural relaxation) are hardly sensitive to chain topology. Its impact, as revealed by this microscopic technique, consists of a slowing down of collective dynamics occurring in the region of the so-called intermediate length scales (ILSs). The ILS region corresponds to length scales larger than the typical intermolecular distances but not yet in the hydrodynamic regime. This is an almost unexplored region in glass-forming systems, and here we apply a recently developed ansatz[24,25] to describe it in the linear precursor melt. In the proposed scenario, a crossover from diffusivelike collective dynamics at intermolecular length scales toward the viscoelastic coupling of stress and density fluctuations at mesoscales is invoked. The behavior of the melt of SCNPs indicates a strong shift of such a crossover to larger length scales. The slower collective dynamics appearing at ILS in the SCNPs—apparently dominated by the slow diffusive component in this framework—is associated with emerging structural heterogeneities with a characteristic length of about 1 nm. We discuss these findings also in the light of recently reported results on macroscopic investigations by rheological and dielectric spectroscopy techniques of these systems.[26]

II. EXPERIMENTAL

A. Samples

Protonated and deuterated SCNPs (hNP and dNP) based on tetrahydrofuran (THF) were obtained from protonated or completely deuterated copolymer precursors (hPrec and dPrec) via intramolecular azide photodecomposition at high dilution conditions. Details about the chemical reactions involved and characterization of hNP and dNP can be found in Refs. 26 and 27. The chemical formula of the deuterated precursor (dPrec) is shown in Fig. 1. The THF-fraction x was 0.81 for hPrec and 0.82 for dPrec. Molecular

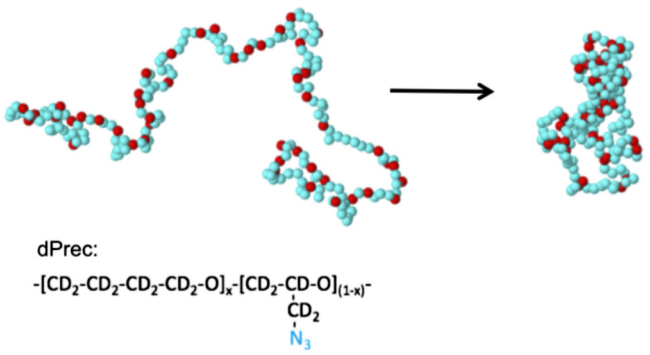

FIG. 1. Schematic representation of the synthesis of a SCNP upon internal cross-linking of a randomly functionalized linear precursor chain. The chemical formula of the deuterated precursor chains is also shown.

weights M_w were 33.2 kg/mol and 36.8 kg/mol with polydispersities M_w/M_n of 1.55 and 1.23 for hPrec and dPrec, respectively. The glass-transition temperatures T_g, 202 K (hPrec) and 199 K (dPrec), increased by 1 K in the corresponding SCNPs' bulk.

B. Neutron scattering experiments

The QENS experiments on the protonated samples were carried out by combining the time-of-flight FOCUS instrument[28] at the Paul Scherrer Institut in Villigen and the SPHERES backscattering spectrometer[29] at the Heinz-Maier-Leibnitz Zentrum in Garching in a finally effective explored Q-range of $0.22 \leq Q \leq 1.84\,\text{Å}^{-1}$. The Neutron Spin Echo (NSE) spectrometer IN11c[30] at the Institute Laue Langevin (ILL) in Grenoble was used to study the dynamic structure factor in the $0.15 \leq Q \leq 1.64\,\text{Å}^{-1}$ range on the deuterated systems.[31] In fully deuterated samples, the scattered neutron intensity is dominated by the coherent contribution, where all atomic pair correlations are approximately equally weighted.[32] Three temperatures well above T_g were investigated for both kinds of samples. Accessing low Q-values, the structural properties at large length scales were explored on the deuterated systems by small angle neutron scattering (SANS) in the D11 instrument at the ILL.[33] The integrated intensity of FOCUS spectra complemented this information for high Q-values in the neighborhood of the amorphous halo.

III. QENS RESULTS: H-SELF-MOTIONS FROM PROTONATED SAMPLES

Figure 2 shows QENS results after Fourier transformation into the time domain and deconvolution from instrumental resolution. The panels on the left correspond to the hPrec sample and on the right to the hNP sample. FOCUS (circles) and SPHERES (diamonds) data are combined.

Nowadays, it is well established[34] that in glass-forming polymers above T_g, the results on protonated samples—corresponding to the intermediate incoherent scattering function of the hydrogens—can be well described above ≈ 2 ps by means of a Kohlrausch–Williams–Watts (KWW) or stretched exponential

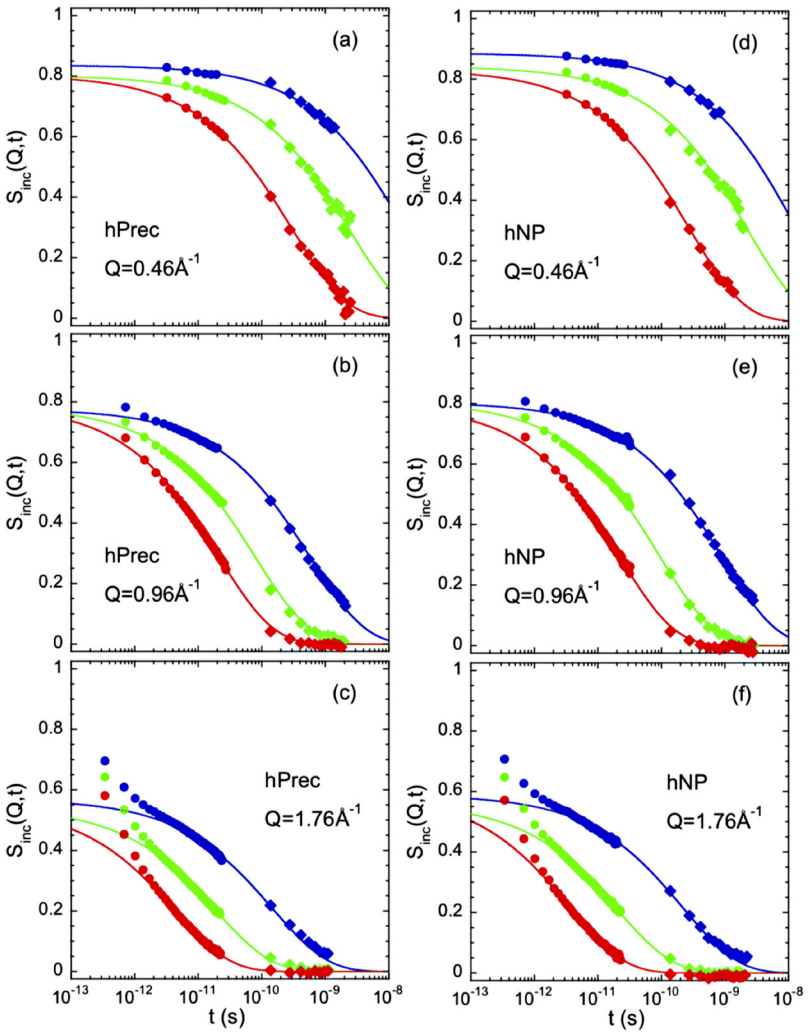

FIG. 2. Fourier transformed and deconvoluted QENS spectra obtained from FOCUS (circles) and SPHERES (diamonds) on the hPrec (a)–(c) and hNP (d)–(f) samples, and the three temperatures investigated: 285 K (blue), 320 K (green), and 360 K (red). The Q-values correspond to 0.46 Å^{-1} (a) and (d), 0.96 Å^{-1} (b) and (e), and 1.76 Å^{-1} (c) and (f). Solid lines are KWW fits with $\beta \equiv 0.5$ to the results above 2 ps.

functional form

$$S_{inc}(Q,t) \propto \exp\left[-\left(\frac{t}{\tau_s}\right)^{\beta}\right], \tag{1}$$

with a stretching exponent β close to 0.5. To check that the melts investigated follow this "standard" behavior, we imposed the constant value of 0.5 for the β-exponent in the fits of the results shown in Fig. 2. As shown, this description works rather well for both sets of data, at least in the accessed dynamic window covered by the experiments. The average characteristic time for H-self-motions $\langle\tau\rangle = \tau_s^H \Gamma(1/\beta)/\beta$, represented in Fig. 3, shows a strong dispersion in Q, being well approximated by a power law $\langle\tau\rangle \propto Q^{-2/\beta}$ (i.e., $\propto Q^{-4}$) in the Q-range $Q \lesssim 1$ Å^{-1}. This relation between dispersion and stretching is indicative of Gaussian diffusive behavior with an associated sublinear increase of the mean squared atomic displacement.[35] Deviations from this asymptotic law at higher Q-values can usually well be accounted for by assuming a distribution of local jumps as the underlying microscopic mechanism for such an anomalous diffusion, which can be resolved by the QENS experiments when exploring small enough length scales.[36,37] In the framework of the anomalous jump diffusion (AJD) model, based on these ideas, the characteristic time for the self-correlation function can be expressed as

$$\tau_s(Q) = \tau_{s,o}\left[1 + \frac{1}{Q^2 \ell_o^2}\right]^{\frac{1}{\beta}}. \tag{2}$$

Here, ℓ_o is the preferred jump length. The resulting values of the parameters involved in the description by this model are provided in Table I. Note that, in this case, hydrogen dynamics is followed by the experiments and consequently, the obtained parameters correspond to these particular nuclei.

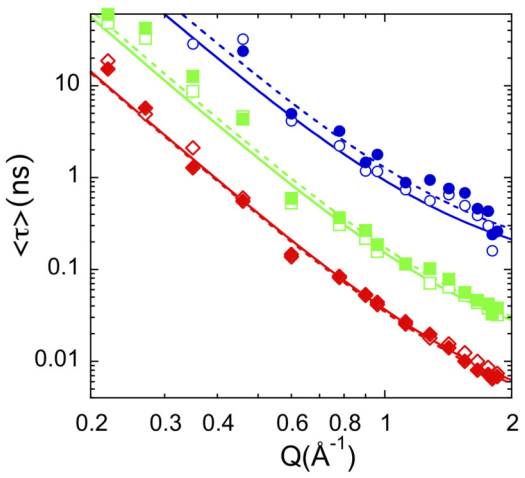

FIG. 3. Scattering vector dependence of the average characteristic time $\langle\tau\rangle = \tau_s^H\Gamma(1/\beta)/\beta$ for H-self motions obtained for hPrec (empty symbols) and hNP (filled symbols) at 285 K (blue circles), 320 K (green squares), and 360 K (red diamonds), imposing $\beta = 0.5$ (fits shown in Fig. 2). Lines are fits of Eq. (2) to the hPrec (solid lines) and hNP (dotted lines) results.

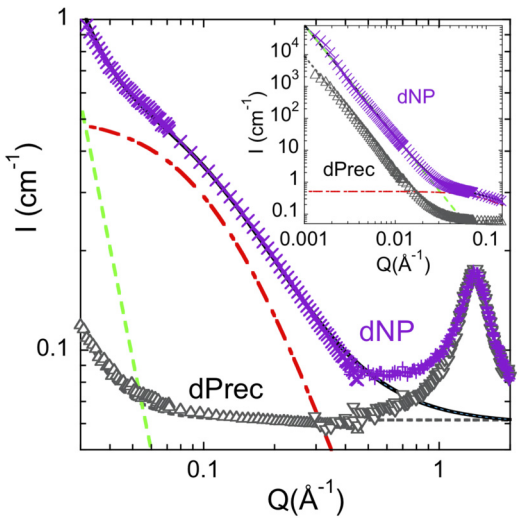

FIG. 4. Differential cross section of dPrec (up-triangles: D11; down-triangles: FOCUS) and dNP (crosses: D11; pluses: FOCUS). The dotted line is a description of the data for dPrec at ILS. The solid line describes the dNP data below ≈ 0.3 Å^{-1}, including an Ornstein–Zernike contribution (dashed–dotted line) and a $\propto Q^{-x}$ law, with $x = 3.5$ (dashed line). The inset shows the low-Q experimental results and contributions for both samples, with the same codes.

IV. COLLECTIVE FEATURES FROM DEUTERATED SAMPLES

The neutron results on the deuterated samples reflect collective features. Figure 4 shows the differential cross section measured on the samples—revealing static properties, in particular, the structure factor $S(Q)$—and in Fig. 5, we can see representative NSE curves representing the normalized dynamic structure factor $S(Q, t)/S(Q)$. We first consider the results corresponding to the linear precursor chains. As can be seen in Fig. 4, the structure factor presents a well defined amorphous halo centered at around $Q_{max} = 1.4$ Å^{-1}. In main-chain polymers, this peak can usually be attributed to correlations between atoms belonging to nearest neighbor chains,[38] separated by an average interchain distance of about $d \approx 2\pi/Q_{max}$. Here, $d \approx 4.5$ Å. To describe the low-Q region of $S(Q)$, a constant function has been considered, as expected for a homogenous system at large length scales with respect to the intermolecular distances. There, long-range density fluctuations are reflected by the structure factor. A low-Q contribution that can be accounted for by a law $\propto Q^{-x}$, with $x = 3.5$, has also been considered. This additional scattering is usually found in fully deuterated polymer melts and could be attributed to the presence of microbubbles. As shown in the inset of the figure, the power law persists down to the lowest-Q values accessed in the SANS experiment.

TABLE I. Values of the parameters involved in the AJD fitting the hPrec results described with KWW functions with $\beta = 0.5$.

T (K)	$\langle\tau_{s,o}^H\rangle$ (ps)	ℓ_o (Å)
285	82	0.64
320	9.4	0.58
360	1.7	0.53

For the intermediate temperature investigated, Fig. 6 shows the NSE results on the normalized $S(Q, t)$ at different Q-values. Let us remind that, for $Q \approx Q_{max}$, these data directly reveal the temporal evolution of interchain correlations. In the terminology of the Mode Coupling Theory (MCT),[39,40] these measurements would constitute the direct microscopic observation of the structural relaxation in the system. As shown in Fig. 6, the curves can be well described by KWW functions

$$\frac{S(Q, t)}{S(Q, 0)} \propto \exp\left[-\left(\frac{t}{\tau_c}\right)^{\beta}\right]. \quad (3)$$

The values obtained for the β parameter are displayed in Fig. 7 as a function of the scattering vector. They show a kind of modulation with the structure factor around an average value of 0.47 for 320 K. With increasing temperature, we observe a tendency of this value to increase, reflecting a less stretched feature of the dynamic structure factor. To determine the characteristic times of the NSE curves, we have assumed a Q-independent β-value equal to the average obtained for each temperature, namely, 0.43 for 280 K, 0.55 for 360 K, and the above reported value of 0.47 for the intermediate temperature. Applying Eq. (3) with these fixed values to all NSE results, the descriptions are good, as can be seen in Figs. 5(a) and 5(b). The average characteristic times obtained are shown as empty symbols in Fig. 8. At high Qs, they show a kind of

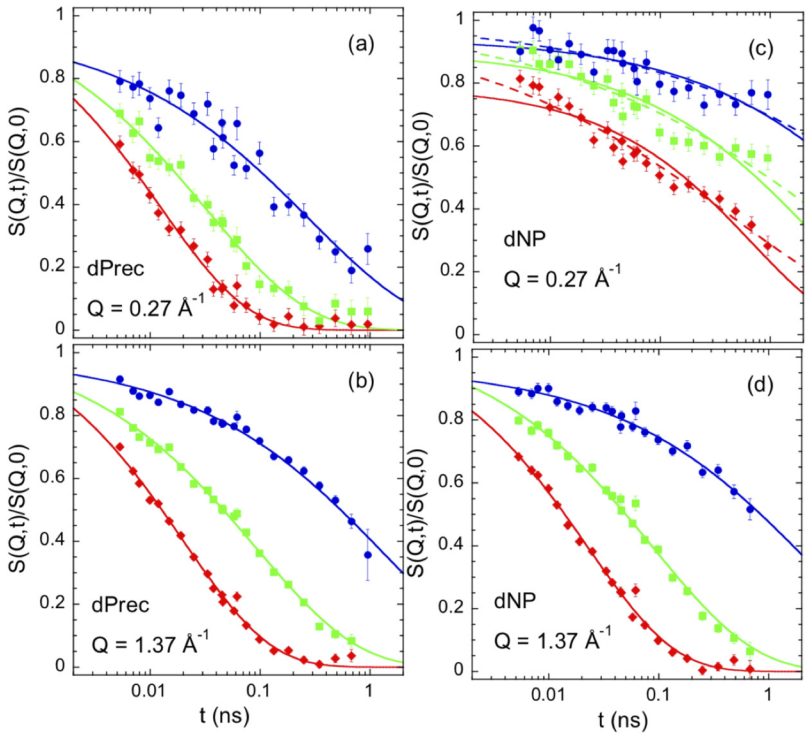

FIG. 5. Normalized dynamic structure factor measured by IN11c at $Q = 0.27\,\text{Å}^{-1}$—i.e., in the ILS region—(upper panels) and at $Q = 1.39\,\text{Å}^{-1}$—i.e., at Q_{max} (lower panels) on dPrec (left panels) and on dNP (right panels) at 280 K (blue circles), 320 K (green squares), and 360 K (red diamonds). Continuous lines are fits of stretched exponentials with $\beta = 0.43$ (280 K), 0.47 (320 K), and 0.55 (360 K), and dashed lines in (c) with $\beta = 0.30$.

maximum reminiscent of the deGennes narrowing proposed for simple diffusion,[41] $\tau_c(Q) \sim S(Q)\tau_s(Q)$.

Approaches merely based on diffusive mechanisms predict for τ_c a continuous slowing down with decreasing scattering vector in the low-Q region well below the structure factor peak. Therefore, they obviously fail in reproducing the experimentally observed acceleration of the collective dynamics at intermediate length scales. Around a given Q_c-value located in the ILS region, the collective response of glass-forming systems crosses over from being dominated by diffusion to a region where it is dominated by the viscoelastic coupling of stress and density fluctuations. Only

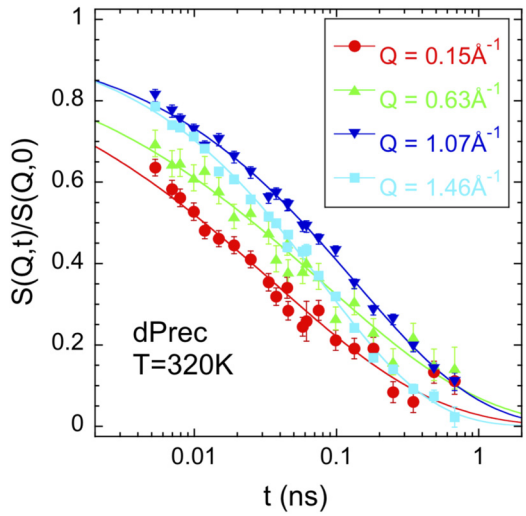

FIG. 6. Normalized dynamic structure factor measured by IN11c at 320 K and the different Q-values indicated. Lines are fits of stretched exponentials with free β-values and prefactor fixed to 0.96.

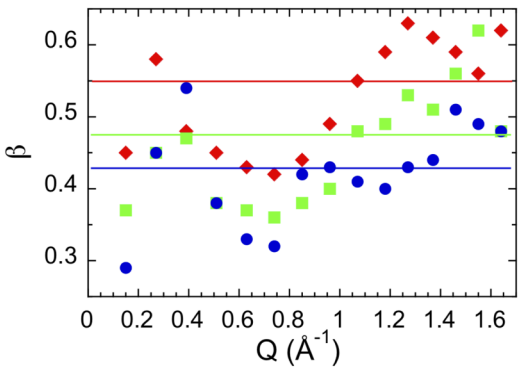

FIG. 7. Scattering vector dependence of the stretching parameter obtained from KWW fits to the dPrec NSE data at 280 K (blue circles), 320 K (green squares), and 360 K (red diamonds). Horizontal lines show the average value for each temperature.

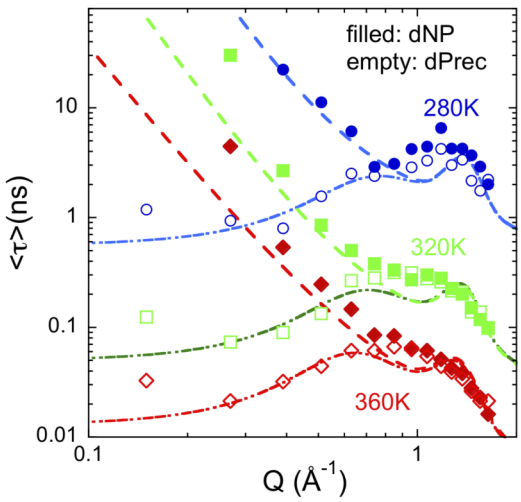

FIG. 8. Q-dependence of the average collective characteristic times $\langle\tau\rangle = \Gamma(1/\beta)\tau_w/\beta$ determined from the NSE experiments (empty symbols: dPrec; filled symbols: dNP) at 280 K (circles, $\beta = 0.43$), 320 K (squares, $\beta = 0.47$), and 360 K (diamonds, $\beta = 0.55$). The dashed-dotted lines are descriptions of the collective times for the precursor in terms of an (anomalous jump) diffusive component (shown as the dashed line for the 280 K case) and a $Q \to 0$ component affected by a cutoff factor (see Appendix).

beyond a certain length scale—somehow related to Q_c—the system would appear as viscoelastically homogeneous. This crossover is captured by a model proposed by Novikov *et al.*[24] that was later reformulated for the case of glass-forming polymers or systems showing stretched relaxation behavior in general.[25] Such an extended approach was applied[25,42,43] to the case of polyisobutylene (PIB) using the NSE data previously reported in Ref. 44. The application of this model to the dPrec results is explained in detail in the Appendix. It provides the description of the collective times shown as dashed-dotted lines in Fig. 8. For the precursor melt, $Q_c \approx 0.6$ Å^{-1}.

We now move to the bulk made of SCNPs. Regarding the local structure, Fig. 4 shows that the amorphous halo of the SCNPs' bulk is exactly in the same position as that of the precursor chains. The average intermolecular distances and short-range order are thus hardly disturbed by internal cross-links. The collective motions involved in the structural relaxation as revealed by NSE in the neighborhood of Q_{max} also take place in a very similar way in the two melts, as can be seen in Figs. 5(b) and 5(d). On the contrary, the decay of the $S(Q, t)$ at ILS is dramatically affected by the presence of intramolecular cross-links. These features are directly evidenced in Fig. 5. While close to Q_{max}, the NSE results on the SCNPs can be very well described by KWW functions with the same β-values as for the melt of precursor chains—and actually with very similar characteristic times—at lower Q-values (below ≈ 0.6 Å^{-1}) the decay becomes more stretched and its characteristic time is longer. As shown in Fig. 5(c) for $Q = 0.27$ Å^{-1}, if still a KWW functional form is imposed, the description of the curves demands lower values of the stretching exponent β. These values decrease with decreasing $Q(\beta(Q \approx 0.5$ Å$^{-1}) \approx 0.4$; $\beta(Q \approx 0.3$ Å$^{-1}) \approx 0.3$; $\beta(Q = 0.15$ Å$^{-1}) \approx 0.2)$. Thus, the SCNP results were analyzed using such Q-dependent β-values (the same for the three temperatures investigated) for $Q \lesssim 0.6$ Å^{-1} and imposing the β-values describing the precursors' data at higher Qs. The average characteristic times obtained in this way are represented in Fig. 8 with filled symbols. For $Q \lesssim 0.6$ Å^{-1}—approaching the ILS—they tend to continuously increase toward larger length scales, reminding a diffusion dominatedlike dynamics in a wide Q-range. In fact, they can be approximately accounted for by the purely diffusive component deduced for dPrec from the previous analysis. In the above commented framework for collective dynamics at ILS, for the melt of SCNPs, the crossover to a nondiffusive characteristic time at Q_c would be strongly shifted to low Q-values (even below those accessed by the IN11c window), implying that the SCNPs bulk would behave viscoelastically homogeneous only at extremely large length scales.

Is there any structural evidence for the existence of heterogeneities responsible for such a dynamical behavior at ILS? SANS experiments provide the answer to this question. As can be seen in Fig. 4, in the Q-region around 0.1 Å^{-1}, SANS results on the melt of SCNPs show indeed a pronounced increase of the scattered intensity with respect to that in the precursor. Such an excess can be well accounted for by an Ornstein-Zernike expression,

$$I_{OZ} \propto \frac{1}{1 + (Q\xi)^2}. \tag{4}$$

A value of about 9 Å for the characteristic length ξ is obtained. To fully describe the SANS results in the whole range investigated, this function is added to a low-Q contribution. The latter follows a similar power law as that found for the melt of precursor chains and might, therefore, be attributed to the same origin—the presence of microbubbles in the samples.

V. DISCUSSION

The dynamics of glass-forming polymers above T_g is very complex and involves different processes and mechanisms for relaxation. The relevance of each of these contributions depends on the length scale of observation. At relatively local length scales of the order of intermolecular distances (equivalently, Q-values in the range 1−2 Å^{-1}), the main dynamical process is the α-relaxation related to the vitrification phenomenon. Let us first focus on the results obtained in such a Q-range. As aforementioned, collective motions reveal nearly identical features for the melt of SCNPs and the melt of linear precursor chains at this level. Regarding the self-motions, the Fourier transformed QENS results on the hNP sample are also very similar to those on hPrec, as can be seen from Fig. 2. After evaluation in terms of the AJD model, we can see in Fig. 3 and Table II that the values of the characteristic times and AJD parameters used to fit them are indistinguishable within the uncertainties. This implies that the atomic motions in the α-relaxation regime can be qualified as corresponding to an anomalous sublinear diffusion with underlying discrete primary steps and are very much the same for both melts.

TABLE II. Values of the parameters involved in the AJD fitting the hNP results described with KWW functions with $\beta = 0.5$.

T (K)	$\langle \tau_{s,o}^{H} \rangle$ (ps)	ℓ_o (Å)
285	103	0.63
320	9.8	0.56
360	1.5	0.51

The differences in the behavior of the two systems start when smaller Q-values (equivalently, larger length scales) are explored. They are clearly patent in the coherent structure factor. The deviations are set in at $Q \approx 0.6$ Å^{-1}. This is the range where also the crossover from α-relaxation to the so-called Rouse dynamics is expected to occur in glass-forming polymers. At large length scales, connectivity plays a crucial role in the dynamics of interconnected objects like macromolecules. The universal predictions of the "bead-spring"-like model proposed by Rouse[45] are expected to describe the dynamics for a melt of linear chains at sufficiently large length scales, as long as entanglement effects are absent (or for times shorter than the entanglement time, for entangled chains). The identification and characterization of the crossover between α-relaxation and Rouse dynamics are nontrivial problems that were subject of studies in the past.[34,46] To check the validity and explore the crossover regime at a microscopic level, two kinds of correlation functions can be used. One of them is the incoherent scattering function corresponding to self-motions of atoms within the segment. This function has been addressed in this work by QENS on hydrogenated polymers. In principle, within the uncertainties, the results on both samples at low-Q values are compatible with the Rouse predictions[45] for incoherent scattering of a KWW functional form with $\beta = 0.5$ and characteristic time following a Q^{-4}-dependence. At the same time, as shown in Fig. 3, the results can also be reasonably described by the extrapolation of the above introduced AJD model toward the lowest Q-values reached. This indicates that, as in other polymers,[22] the crossover between both dynamical regimes takes place in a very subtle way and it is not easy to clearly define their limits. A detailed scrutiny of this crossover is beyond the scope of this work, where we want to focus on the impact of the cross-links on the observed dynamical features. Conversely, due to the strong Q-dependence of the incoherent scattering in the low Q-regime and the limited energy resolution of the spectrometers, the accuracy in the determination of the characteristic times prevents a precise quantification of their differences. From a direct comparison of the FOCUS results at low Q-values, a small difference could be envisaged between the two melts (see Fig. 9). The spectra corresponding to the SCNPs are slightly narrower, pointing to a subtly slower dynamics at large length scales.

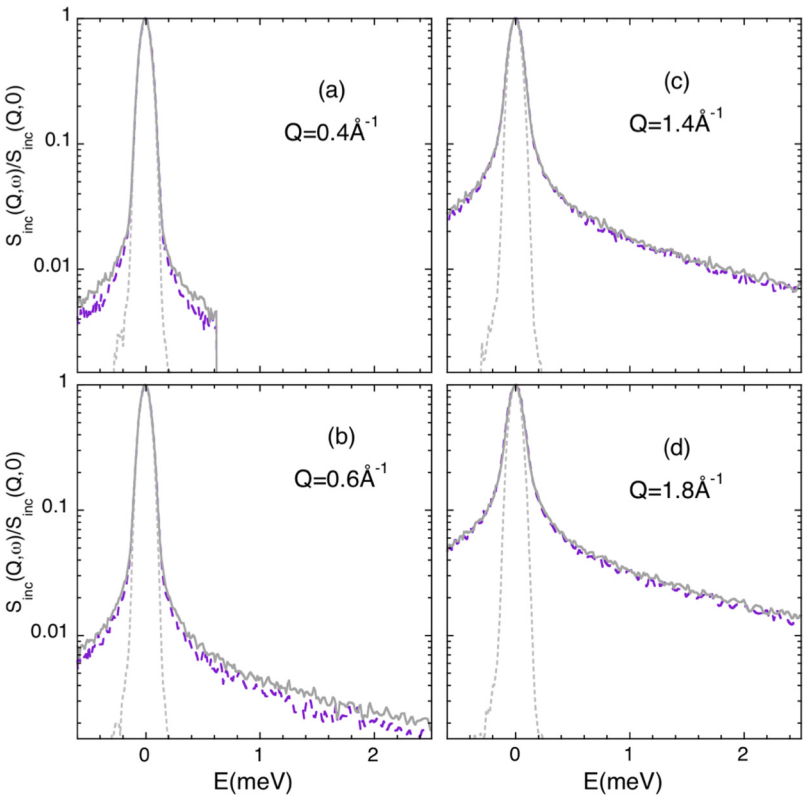

FIG. 9. Normalized FOCUS spectra obtained at 320 K and the different Q-values indicated for hPrec (solid line) and hNP (dashed line). The dotted line shows the instrumental resolution function.

The other correlation function for which the Rouse model formulation is provided is the single chain dynamic structure factor. This is available by NSE on labeled samples where hydrogenated and deuterated chains are mixed and relates to pairs of atoms intramolecularly connected. Studies on such melts of polymers have demonstrated the validity of the Rouse model in its range of applicability.[34] This is, however, severely limited for long chains at long times. Long linear chains can easily interpenetrate. At long times, the topological constraints emerging from interpenetration together with chain uncrossability—the entanglements—lead to deviations from standard Rouse-like dynamics that can be accounted for invoking the tube concept and related reptation mechanism proposed by deGennes and Edwards.[34] The single-chain dynamic structure factor of the melts here investigated will be the subject of future work, where we will address the impact of intramolecular cross-linking on the entanglement formation with a direct microscopic insight. Here, we comment that in a recent work[26] including a rheological study of the melts here presented, an almost complete disappearance of the rubbery plateau has been found for the melt of SCNPs with respect to the precursor system. Such a striking effect suggests a strong suppression of the entanglements and was attributed to the internal multiloop topology of the SCNPs.[47–49] It is well known that, in ring polymers, the entanglement formation is strongly hindered with respect to their linear counterparts.[50–52]

In the present paper, the NSE experiments were carried out on fully deuterated samples. They thus address the collective features involving all atomic pair correlations, independently of belonging to the same or different chains. There is no theoretical framework that expresses the accessed observable—the dynamic structure factor—in terms of the Rouse model or similar approaches considering chain dynamics as key ingredients. We have thus applied a recently proposed ansatz to describe the reference results on the dPrec melt sample. It is worth noting that such an approach had only been considered until now for the case of PIB and seems to work reasonably well also for PTHF from the present study. In this framework, the NSE results on the SCNPs point to a strong shift of the crossover to viscoelastically homogeneous behavior toward much larger length scales than in the linear precursors. In fact, our SANS experiments show that internal cross-linking induces an excess of density fluctuations at nanometric length scales with respect to the melt of linear topology. The presence of cross-links also manifests in a more complex relaxation of the dynamic structure factor at such length scales. Its functional form becomes markedly more stretched than in the melt of linear chains and the characteristic times increase dramatically with decreasing Q-value—at least in the window covered by the NSE experiments. These effects could be attributed to the emergence of new constraints in the SCNPs melt related to the internal domain topology and leading to certain correlations to persist over longer times. Additional mechanisms for relaxation would thus need to appear in the internally cross-linked melt in order to reach the complete decay of the dynamic structure factor. Close to cross-links and, in particular, within small domains, chain conformation and packing would differ from the average in the bulk material. Neighboring segments chemically connected by the internal cross-links induced during SCNPs synthesis could feel an extra friction to relax, provoking the retardation of the decay of the density fluctuations at the corresponding length scales. The topological complexity induced by intramolecular bonding would be expected to require the occurrence of a hierarchy of relaxation mechanisms to reach the full relaxation of the SCNPs in the melt. In fact, the dielectric spectroscopy investigation reported in the above referred work[26] points to the appearance of an additional dynamic contribution to dipolar relaxation slower than the α-process that would be related to the relaxation mechanism involving the internal domains in the SCNPs.

Finally, we compare our results on the melt of SCNPs with those previously obtained on nanocomposites consisting of mixtures of poly(methyl methacrylate) (PMMA)-based SCNPs and linear chains of polyethylene oxide (PEO).[21–23] In those works, the mutual influence of both components on the dynamics was addressed by neutron scattering on labeled samples. Due to limitations of the experimental window, the most thorough studies were carried out on the PEO component. For this component, a shift in the glass-transition temperature revealing slower segmental dynamics as well as a slowdown of the Rouse modes was observed upon mixing with the more rigid SCNPs. These effects were also found in blends of the linear counterparts and can in principle be attributed to the large dynamic asymmetry displayed by the two components of the mixture; therefore, they would not be expected in our SCNPs melt, where all the structural units are chemically identical. We find, nevertheless, hints for slowdown and stretching of the dynamical response at large length scales that are not related to enhanced intermolecular friction due to a neighboring more rigid component. On the other hand, the main effect observed when the topology of the PMMA-like component in the nanocomposite changes from a linear chain to a SCNP is a striking tube dilation for PEO chain dynamics. As shown by the rheological measurements on the SCNPs melt above commented,[26] an effective disentanglement is also observed upon internal cross-linking of the PTHF chains. Thus, the creation of internal loops in the macromolecules seems to induce a release of the topological constraints for chain dynamics in both kinds of systems, despite their very different intrinsic properties.

VI. CONCLUSIONS

SCNPs are fascinating nano-objects not only for their potential use in a large variety of fields in the nanotechnology arena, but also as model systems to investigate fundamental problems of polymer dynamics. In particular, here we have addressed the question of how intramolecular cross-linking affects the atomic motions and the collective features at length scales of the order of the intermolecular distances and larger, exploring the regime of the so-called intermediate length scales region. With this aim, we have performed a parallel investigation on the melt composed by linear chains as a reference. For this reference sample, we have found "standard" self-motions describable by the anomalous jump diffusion model in the whole Q-range investigated, pointing thus to a very smooth crossover from α-relaxation toward Rouse-like dynamics. We have also shown that the recently proposed ansatz to describe the collective dynamics at ILS for glass-forming polymers[25] based on that developed by Novikov *et al.*[24] works rather well for the linear precursor melt. We note that this kind of

investigation is very scarce in the literature and, therefore, this work has also contributed in this direction. The impact of intramolecular cross-linking is hardly resolvable at length scales of the order of the intermolecular average distances as microscopically explored by both the dynamic structure factor and the incoherent scattering function of hydrogens addressed by our quasielastic neutron scattering experiments. The effects set in at larger length scales, toward the intermediate length scales regime, where also the crossover from segmental to Rouse dynamics is expected. A subtle slowdown of the hydrogen self-motions can be inferred from the low-Q results on the hNP-samples. The main effect is observed on the coherent scattering: structural heterogeneities are revealed by SANS, and the decay of the dynamic structure factor exhibits marked extra-stretching as well as much longer characteristic times than the precursor melt. The emergence of a hierarchy of complex additional mechanisms for the relaxation of internal loops in the SCNPs would be at the origin of these observations for collective dynamics. Future experiments on the single chain dynamic structure factor (isotopically labeled macromolecules in a melt of SCNPs) may elucidate the impact of intramolecular cross-links on chain dynamics at a molecular level for these intriguing systems.

ACKNOWLEDGMENTS

We acknowledge the financial support of the Basque Government (Code No. IT-1175-19) and the Ministerio de Economía y Competitividad [Code No. PGC2018-094548-B-I00 (MCIU/AEI/FEDER, UE)]. This work was based on experiments performed at the FOCUS instrument operated by the Swiss spallation neutron source SINQ (Paul Scherrer Institute, Villigen, Switzerland) and SPHERES [Heinz–Maier–Leibnitz Zentrum (MLZ), Garching, Germany] and was supported by the European Commission under the 7th Framework Programme through the "Research Infrastructures" action of the "Capacities" Programme, NMI3-II (Grant No. 283883).

APPENDIX: MODEL TO DESCRIBE THE COLLECTIVE RELAXATION AT MESOSCALES IN GLASS-FORMING SYSTEMS—APPLICATION TO THE LINEAR PRECURSOR MELT

The window spanned by NSE in our experiments covers the neighborhood of the structure factor peak and the so-called intermediate length scales regime. A model has been recently proposed to describe the collective dynamics of glass-forming polymers there and successfully applied to the case of existing data on polyisobutylene (PIB).[25,42,43] This model consists of an interpolation formula that embeds the mesoscopic (nondiffusive) and the high-Q (diffusive) limits of the collective times in an analytical expression as proposed by Novikov *et al.*,[24]

$$\frac{1}{\tau_c(Q)} = \frac{1}{\tau_c^{Q\to 0}} e^{-Q^2\xi_c^2} + \frac{1}{\tau_c^D(Q)}. \tag{A1}$$

The nondiffusive (Q-independent) time $\tau_c^{Q\to 0}$ should reflect the viscoelastic coupling of stress and density fluctuations on scales long enough compared to atomic dimensions, but not yet in the hydrodynamic limit.[24] Its contribution to the total collective time is affected by a Gaussian cutoff factor $e^{-Q^2\xi_c^2}$ to ensure that it is present only on length scales beyond a characteristic length ξ_c. This characteristic length is expected to be $\xi_c \sim 2\pi/Q_{max}$. On the other hand, the collective diffusive time $\tau_c^D(Q)$ can be obtained in the spirit of a Sköld[53]-like renormalization,

$$\frac{S(Q,t)}{S(Q,0)} \approx S_{inc}\left(\frac{Q}{\sqrt{S(Q)}}, t\right). \tag{A2}$$

The approximation for the diffusive contribution was generalized to the case of the observed anomalous diffusion. In particular, to account for the full phenomenology observed for glass-forming polymers, the incoherent scattering function was assumed to be that corresponding to the AJD model above introduced, i.e., Eq. (1) together with the expression for the characteristic time [Eq. (2)]. Then, the collective diffusive counterpart of $\tau_s(Q)$ can be expressed as

$$\tau_c^D(Q) = \tau_{s,o}\left[1 + \frac{S(Q)}{Q^2\ell_o^2}\right]^{\frac{1}{\beta}}. \tag{A3}$$

The model for collective times of the precursor was applied using the information on self-atomic motions obtained by QENS on the protonated sample. Figures 10 and 11 show the experimental times obtained using the same Q-independent β-parameter to fit both correlation functions. It was chosen as the one better describing on average the collective results. The solid lines in Fig. 10 are fits of the hydrogen self-correlation times to Eq. (2). The resulting parameters are given in Table III. We note that the characteristic time $\tau_s(Q)$ involved in the calculation of τ_c^D corresponds to the self-part of the dynamic structure factor, in which all

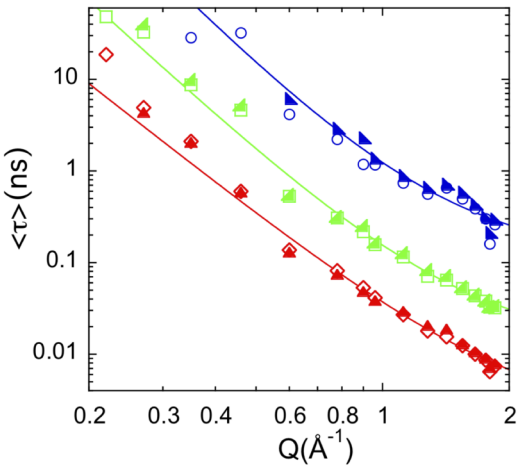

FIG. 10. Scattering vector dependence of the average characteristic time $\langle\tau\rangle = \tau_s^H\Gamma(1/\beta)/\beta$ for H-self motions obtained for hPrec using $\beta \equiv 0.5$ (empty symbols, same as in Fig. 3) and the same β-value as for describing the NSE results (filled symbols). Lines are fits of Eq. (2) to the latter.

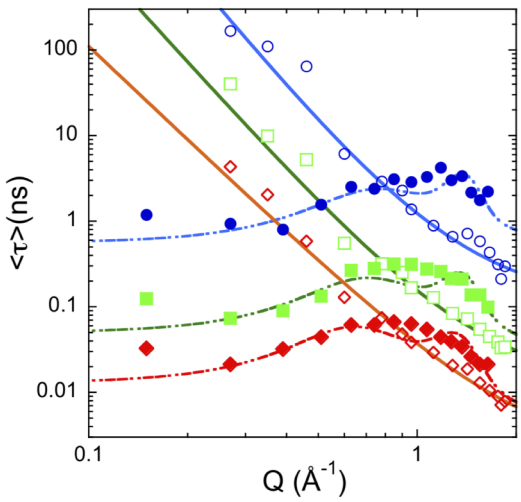

FIG. 11. Collective characteristic times measured on dPrec (filled symbols) and characteristic times for H-self motions determined from the QENS experiments on hPrec (empty symbols) for the three temperatures investigated: the red diamonds correspond to 360 K, the green squares correspond to 320 K, and the blue circles correspond to 280 K (dPrec) and 285 K (hPrec). Solid lines are fits of Eq. (2) to the incoherent times and dashed-dotted lines of the model for collective times.

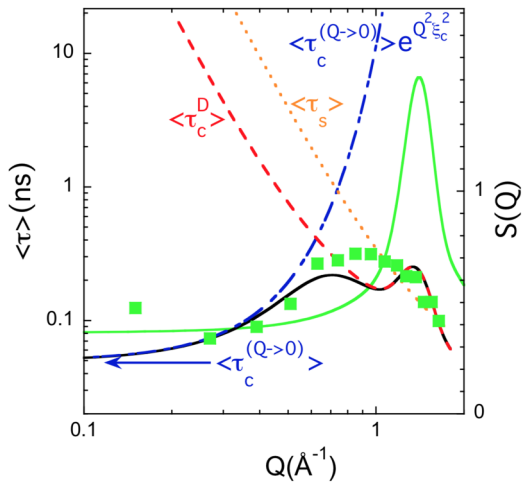

FIG. 12. Illustration of the components of the model for collective dynamics to the case of the precursor melt at 320 K (symbols: experimental results; black solid line: total fitting curve). The dashed-dotted line is the mesoscopic contribution (affected by the cutoff factor), and the dashed line is the diffusive component. Its self-counterpart is represented by the dotted line. The arrow indicates the value of the asymptotic $\tau_c^{Q\to 0}$-value. The structure factor function is also shown as the green solid line.

nuclei, not only the hydrogens, are involved. Therefore, it might differ from the characteristic time experimentally determined from QENS measurements on protonated samples. In fact, in the case of PIB, where molecular dynamics simulations were available, a proportionality factor was found to be about 2 between $\tau_s(Q)$ calculated averaging overall the nuclei and $\tau_s^H(Q)$. Therefore, we have assumed that $\tau_c^D(Q)$ can be approximated by Eq. (A3) with the same ℓ_o as that determined for $\tau_s^H(Q)$ and $\tau_{s,o} = A\tau_{s,o}^H$ (for the collective results at 280 K, the information extracted from the QENS measurements on the protonated sample at 285 K was used). Then, the only free parameters involved in the application of the model [combining Eqs. (A1) and (A3)] were A, $\langle\tau_c^{Q\to 0}\rangle$, and ξ_c. The resulting fitting curves are shown by the dashed-dotted lines in Fig. 11, and the values of the parameters are listed in Table III. For illustrating the model, in Fig. 12, the two contributions to the total model curve are represented: that from the mesoscopic time (indicated by the arrow) affected by the cutoff factor, and the collective (anomalous) diffusive characteristic time. The implicitly used self-correlation time is also depicted.

TABLE III. Values of the parameters involved in the application of the model.

T (K)	β	$\langle\tau_{s,o}^H\rangle$ (ps)	ℓ_o (Å)	A	$\langle\tau_c^{Q\to 0}\rangle$ (ps)	ξ_c (Å)
285	0.43	105	0.73	…	…	…
280	0.43	…	…	4.4	560	2.2
320	0.47	11.3	0.64	2.2	50	2.3
360	0.55	1.8	0.48	1.7	13	2.6

REFERENCES

[1] *Single-Chain Polymer Nanoparticles: Synthesis, Characterization, Simulations, and Applications*, edited by J. A. Pomposo (John Wiley & Sons, Weinheim, Germany, 2017).

[2] J. Rubio-Cervilla, E. González, and J. A. Pomposo, "Advances in single-chain nanoparticles for catalysis applications," Nanomaterials **7**, 341 (2017).

[3] A. Sanchez-Sanchez, A. Arbe, J. Colmenero, and J. A. Pomposo, "Metallo-folded single-chain nanoparticles with catalytic selectivity," ACS Macro Lett. **3**, 439–443 (2014).

[4] H. Rothfuss, N. D. Knöfel, P. W. Roesky, and C. Barner-Kowollik, "Single-chain nanoparticles as catalytic nanoreactors," J. Am. Chem. Soc. **140**, 5875–5881 (2018).

[5] J. He, L. Tremblay, S. Lacelle, and Y. Zhao, "Preparation of polymer single chain nanoparticles using intramolecular photodimerization of coumarin," Soft Matter **7**, 2380–2386 (2011).

[6] G. Qian, B. Zhu, Y. Wang, S. Deng, and A. Hu, "Size-tunable polymeric nanoreactors for one-pot synthesis and encapsulation of quantum dots," Macromol. Rapid Commun. **33**, 1393–1398 (2012).

[7] A. Sanchez-Sanchez, A. Arbe, J. Kohlbrecher, J. Colmenero, and J. A. Pomposo, "Efficient synthesis of single-chain globules mimicking the morphology and polymerase activity of metalloenzymes," Macromol. Rapid Commun. **36**, 1592–1597 (2015).

[8] J. De-La-Cuesta, I. Asenjo-Sanz, A. Latorre-Sánchez, E. González, D. E. Martínez-Tong, and J. A. Pomposo, "Enzyme-mimetic synthesis of PEDOT from self-folded iron-containing single-chain nanoparticles," Eur. Polym. J. **109**, 447–452 (2018).

[9] B. Zhu, S. Sun, Y. Wang, S. Deng, G. Qian, M. Wang, and A. Hu, "Preparation of carbon nanodots from single chain polymeric nanoparticles and theoretical investigation of the photoluminescence mechanism," J. Mater. Chem. C **1**, 580–586 (2013).

[10] W. Fan, X. Tong, F. Farnia, B. Yu, and Y. Zhao, "CO_2-responsive polymer single-chain nanoparticles and self-assembly for gas-tunable nanoreactors," Chem. Mater. **29**, 5693–5701 (2017).

[11]M. A. J. Gillissen, I. K. Voets, E. W. Meijer, and A. R. A. Palmans, "Single chain polymeric nanoparticles as compartmentalised sensors for metal ions," Polym. Chem. **3**, 3166–3174 (2012).
[12]A. Latorre-Sanchez and J. A. Pomposo, "A simple, fast and highly sensitive colorimetric detection of zein in aqueous ethanol via zein–pyridine–gold interactions," Chem. Commun. **51**, 15736–15738 (2015).
[13]C. T. Adkins, J. N. Dobish, S. Brown, and E. Harth, "Water-soluble semiconducting nanoparticles for imaging," ACS Macro Lett. **2**, 710–714 (2013).
[14]A. B. Benito, M. K. Aiertza, M. Marradi, L. Gil-Iceta, T. Shekhter Zahavi, B. Szczupak, M. Jiménez-González, T. Reese, E. Scanziani, L. Passoni, M. Matteoli, M. De Maglie, A. Orenstein, M. Oron-Herman, G. Kostenich, L. Buzhansky, E. Gazit, H.-J. Grande, V. Gómez-Vallejo, J. Llop, and I. Loinaz, "Functional single-chain polymer nanoparticles: Targeting and imaging pancreatic tumors in vivo," Biomacromolecules **17**, 3213–3221 (2016).
[15]J. De-La-Cuesta, E. González, and J. A. Pomposo, "Advances in fluorescent single-chain nanoparticles," Molecules **22**, 1819 (2017).
[16]G. Njikang, G. Liu, and L. Hong, "Chiral imprinting of diblock copolymer single-chain particles," Langmuir **27**, 7176–7184 (2011).
[17]S. K. Hamilton and E. Harth, "Molecular dendritic transporter nanoparticle vectors provide efficient intracellular delivery of peptides," ACS Nano **3**, 402–410 (2009).
[18]A. Sanchez-Sanchez, S. Akbari, A. Etxeberria, A. Arbe, U. Gasser, A. J. Moreno, J. Colmenero, and J. A. Pomposo, ""Michael" nanocarriers mimicking transient-binding disordered proteins," ACS Macro Lett. **2**, 491–495 (2013).
[19]C.-C. Cheng, D.-J. Lee, Z.-S. Liao, and J.-J. Huang, "Stimuli-responsive single-chain polymeric nanoparticles towards the development of efficient drug delivery systems," Polym. Chem. **7**, 6164–6169 (2016).
[20]B. Robles-Hernández, X. Monnier, J. A. Pomposo, M. Gonzalez-Burgos, D. Cangialosi, and A. Alegría, "Glassy dynamics of an all-polymer nanocomposite based on polystyrene single-chain nanoparticles," Macromolecules **52**, 6868–6877 (2019).
[21]D. Bhowmik, J. A. Pomposo, F. Juranyi, V. García Sakai, M. Zamponi, A. Arbe, and J. Colmenero, "Investigation of a nanocomposite of 75 wt.% poly (methyl methacrylate) nanoparticles with 25 wt.% poly(ethylene oxide) linear chains: A quasielatic neutron scattering, calorimetric, and waxs study," Macromolecules **47**, 3005–3016 (2014).
[22]D. Bhowmik, J. A. Pomposo, F. Juranyi, V. García-Sakai, M. Zamponi, Y. Su, A. Arbe, and J. Colmenero, "Microscopic dynamics in nanocomposites of poly(ethylene oxide) and poly(methyl methacrylate) soft nanoparticles: A quasi-elastic neutron scattering study," Macromolecules **47**, 304–315 (2014).
[23]A. Arbe, J. A. Pomposo, I. Asenjo-Sanz, D. Bhowmik, O. Ivanova, J. Kohlbrecher, and J. Colmenero, "Single chain dynamic structure factor of linear polymers in an all-polymer nano-composite," Macromolecules **49**, 2354–2364 (2016).
[24]V. N. Novikov, K. S. Schweizer, and A. P. Sokolov, "Coherent neutron scattering and collective dynamics on mesoscale," J. Chem. Phys. **138**, 164508 (2013).
[25]J. Colmenero, F. Alvarez, Y. Khairy, and A. Arbe, "Modeling the collective relaxation time of glass-forming polymers at intermediate length scales: Application to polyisobutylene," J. Chem. Phys. **139**, 044906 (2013).
[26]A. Arbe, J. Rubio-Cervilla, A. Alegría, A. J. Moreno, J. A. Pomposo, B. Robles-Hernández, P. Malo de Molina, P. Fouquet, F. Juranyi, and J. Colmenero, "Mesoscale dynamics in melts of single-chain polymeric nanoparticles," Macromolecules **52**, 6935–6942 (2019).
[27]J. Rubio-Cervilla, P. Malo de Molina, B. Robles-Hernández, A. Arbe, A. J. Moreno, A. Alegría, J. Colmenero, and J. A. Pomposo, "Facile access to completely deuterated single-chain nanoparticles enabled by intramolecular azide photodecomposition," Macromol. Rapid Commun. **40**, 1900046 (2019).
[28]S. Jansen, J. Mesot, L. Holitzner, A. Furrer, and R. Hempelmann, "Focus: A hybrid TOF-sectrometer at SINQ," Physica B **234–236**, 1174–1176 (1997).
[29]J. Wuttke, A. Budwig, M. Drochner, H. Kämmerling, F.-J. Kayser, H. Kleines, V. Ossovyi, L. C. Pardo, M. Prager, D. Richter, G. J. Schneider, H. Schneider, and S. Staringer, "Spheres, Jülich's high-flux neutron backscattering spectrometer at FRM II," Rev. Sci. Instrum. **83**, 075109 (2012).
[30]B. Farago, "IN11C, medium-resolution multidetector extension of the IN11 NSC spectrometer at the ILL," Physica B **241–243**, 113–116 (1998).
[31]Institut Laue Langevin, Grenoble, see http://dx.doi.org/10.5291/ILL-DATA.6-04-275.
[32]S. W. Lovesey, *Theory of Neutron Scattering from Condensed Matter* (Clarendon Press, Oxford, 1984).
[33]Institut Laue Langevin, Grenoble, see https://doi.ill.fr/10.5291/ILL-DATA.9-11-1833.
[34]D. Richter, M. Monkenbusch, A. Arbe, and J. Colmenero, *Neutron Spin Echo in Polymer Systems*, Advances in Polymer Sciences Vol. 174 (Springer Verlag, Berlin Heidelberg New York, 2005).
[35]J. Colmenero, A. Alegría, A. Arbe, and B. Frick, "Correlation between non-Debye behavior and Q behavior of the α relaxation in glass-forming polymeric systems," Phys. Rev. Lett. **69**, 478–481 (1992).
[36]A. Arbe, J. Colmenero, F. Alvarez, M. Monkenbusch, D. Richter, B. Farago, and B. Frick, "Non-Gaussian nature of the α relaxation of glass-forming polyisoprene," Phys. Rev. Lett. **89**, 245701 (2002).
[37]A. Arbe, J. Colmenero, F. Alvarez, M. Monkenbusch, D. Richter, B. Farago, and B. Frick, "Experimental evidence by neutron scattering of a crossover from Gaussian to non-Gaussian behavior in the α relaxation of polyisoprene," Phys. Rev. E **67**, 051802 (2003).
[38]B. Frick, D. Richter, and C. Ritter, "Structural changes near the glass transition–neutron diffraction on a simple polymer," Europhys. Lett. **9**, 557–562 (1989).
[39]W. Götze and L. Sjögren, "Relaxation processes in supercooled liquids," Rep. Prog. Phys. **55**, 241–376 (1992).
[40]W. Götze, *Complex Dynamics of Glass-Forming Liquids. A Mode Coupling Theory* (Oxford University Press, New York, 2009).
[41]P. D. Gennes, "Liquid dynamics and inelastic scattering of neutrons," Physica **25**, 825–839 (1959).
[42]J. Colmenero, F. Alvarez, and A. Arbe, "Collective dynamics of glass-forming polymers at intermediate length scales—A synergetic combination of neutron scattering, atomistic simulations and theoretical modelling," EPJ Web Conf. **83**, 01001 (2015).
[43]Y. Khairy, F. Alvarez, A. Arbe, and J. Colmenero, "Collective features in polyisobutylene. A study of the static and dynamic structure factor by molecular dynamics simulations," Macromolecules **47**, 447–459 (2014).
[44]B. Farago, A. Arbe, J. Colmenero, R. Faust, U. Buchenau, and D. Richter, "Intermediate length scale dynamics of polyisobutylene," Phys. Rev. E **65**, 051803 (2002).
[45]P. E. J. Rouse, "A theory of the linear viscoelastic properties of dilute solutions of coiling polymers," J. Chem. Phys. **21**, 1272–1280 (1953).
[46]D. Richter, M. Monkenbusch, L. Willner, A. Arbe, J. Colmenero, and B. Farago, "Direct observation of the crossover from α-relaxation to rouse dynamics in a polymer melt," Europhys. Lett. **66**, 239–245 (2004).
[47]A. J. Moreno, F. Lo Verso, A. Sanchez-Sanchez, A. Arbe, J. Colmenero, and J. A. Pomposo, "Advantages of orthogonal folding of single polymer chains to soft nanoparticles," Macromolecules **46**, 9748–9759 (2013).
[48]A. J. Moreno, F. Lo Verso, A. Arbe, J. A. Pomposo, and J. Colmenero, "Concentrated solutions of single-chain nanoparticles: A simple model for intrinsically disordered proteins under crowding conditions," J. Phys. Chem. Lett. **7**, 838–844 (2016).
[49]J. A. Pomposo, A. J. Moreno, A. Arbe, and J. Colmenero, "Local domain size in single-chain polymer nanoparticles," ACS Omega **3**, 8648–8654 (2018).
[50]D. Vlassopoulos, "Macromolecular topology and rheology: Beyond the tube model," Rheol. Acta **55**, 613–632 (2016).
[51]J. D. Halverson, W. B. Lee, G. S. Grest, A. Y. Grosberg, and K. Kremer, "Molecular dynamics simulation study of nonconcatenated ring polymers in a melt. I. Statics," J. Chem. Phys. **134**, 204904 (2011).
[52]A. Rosa and R. Everaers, "Ring polymers in the melt state: The physics of crumpling," Phys. Rev. Lett. **112**, 118302 (2014). (1–5)
[53]K. Sköld, "Small energy transfer scattering of cold neutrons from liquid argon," Phys. Rev. Lett. **19**, 1023–1025 (1967).